

# Cholesterol effect on the specific capacitance of sub-micrometric DOPC bilayer patches measured by in-liquid scanning dielectric microscopy

*Martina Di Muzio<sup>1,2</sup>, Ruben Millan-Solsona<sup>1,2</sup>, Jordi H. Borrell<sup>3,4</sup>, Laura Fumagalli<sup>5,6</sup>, Gabriel Gomila<sup>\*1,2</sup>*

<sup>1</sup>Nanoscale Bioelectrical Characterization, Institut de Bioenginyeria de Catalunya, The Barcelona Institute of Science and Technology, 08028, Barcelona, Spain

<sup>2</sup>Departament d'Enginyeria Electrònica i Biomèdica, Universitat de Barcelona, 08028, Barcelona, Spain

<sup>3</sup>Secció de Fisicoquímica, Facultat de Farmàcia i Ciències de l'Alimentació, Universitat de Barcelona, 08028, Barcelona, Spain

<sup>4</sup>Institute of Nanoscience and Nanotechnology, Universitat de Barcelona, 08028, Barcelona, Spain

<sup>5</sup>School of Physics and Astronomy, University of Manchester, Manchester M13 9PL, UK

<sup>6</sup>National Graphene Institute, University of Manchester, Manchester M13 9PL, UK

KEYWORDS: Specific capacitance, lipid bilayers, cholesterol, in-liquid scanning dielectric microscopy, nanoscale dielectric properties.

ABSTRACT. The specific capacitance of biological membranes is a key physical parameter in bioelectricity that also provides valuable physicochemical information on composition, phase or hydration properties. Cholesterol is known to modulate the physicochemical properties of biomembranes, but its effect on the specific capacitance has not been fully established, yet. Here we use the high spatial resolution capabilities of in-liquid Scanning Dielectric Microscopy in force detection mode to directly demonstrate that DOPC bilayer patches at 50% cholesterol concentration show a strong reduction of their specific capacitance with respect to pure DOPC bilayer patches. The reduction observed (~35%) cannot be explained by the small increase in bilayer thickness (~16%). We suggest that the reduction of the specific capacitance might be due to the dehydration of the polar head groups caused by the insertion of cholesterol molecules in the bilayer. The results reported confirm the potential of in-liquid SDM to study the electrical and physicochemical properties of lipid bilayers at very small scales (down to ~200 nm here), with implications in fields such as biophysics, bioelectricity, biochemistry and biosensing.

## INTRODUCTION

The specific capacitance of biological membranes determines the charge per unit of area that accumulates on their sides in response to a membrane voltage difference ( $V$ ). It constitutes a key physical parameter in bioelectricity, since it determines the ions and charged molecules partitioning into the cell membrane and the very low membrane ionic conductivity (2), the charging time and propagation velocity of action potentials ( $V$ ), the voltage thresholds for cell membrane electroporation (3) or the level of screening in the electrostatic interaction of

biomolecules with cell membranes (4). It also determines the cell response to external electric fields relevant in bioimpedance measurements (5) and in electrokinetic techniques such as dielectrophoresis (6) or electrorotation (7).

The specific capacitance of membranes depends on their thickness,  $d_m$ , and electric polarization properties (i.e. its relative dielectric constant,  $\epsilon_m$ ), through the relationship  $c_m = \epsilon_0 \epsilon_m / d_m$ , where  $\epsilon_0$  is the vacuum permittivity. Any factor affecting any one of these two parameters (thickness and/or dielectric constant) influences the value of the membrane specific capacitance. Examples include the membrane composition (8), (9), (10), phase state (11), (12), (13), temperature (13) or solution pH (14), among others. The specific capacitance is, then, a powerful physicochemical membrane reporter, with the main advantage with respect to environmental sensitive fluorescence probes (15), (16) or spin paramagnetic resonance probes (17), (18), (19), of being determined by intrinsic properties, and, hence, not requiring of exogenous probes.

Cholesterol is known to modulate the physicochemical properties of biomembranes, but its effect on the specific capacitance of biomembranes has not been fully established, yet. Cholesterol (chol) is the main sterol biosynthesized by animal cells and its presence is essential for many membrane's associated processes since it can modulate membrane properties such as lipid diffusivity, stiffness or dipole moment (20). Cholesterol has been reported to increase (8), (21), (22), (23) or decrease (24), (25), (26) the specific capacitance of biomembranes, and in some cases an increase or decrease depending on the cholesterol concentration (27). These discrepancies have been attributed, most often, to sample preparation methods (e.g. presence of solvent on the bilayers), but, also, to a limited accuracy and reproducibility of existing measuring techniques (28).

A variety of electrical techniques and methods have been developed over the years to measure the specific capacitance of biomembranes. For natural cell membranes, one finds electrorotation measurements on single suspended cells (29) and current/voltage time varying measurements with micropipette electrodes attached to cells (30), (31) or to cell detached membrane patches (32). For synthetic membranes (such as model lipid bilayers), measurements have been mostly performed by current/voltage time varying techniques on membranes suspended on small apertures (e.g. black lipid bilayers) (33) or supported on planar solid electrodes (34), (35) (see Ref. (28) for a review). Efforts have been devoted to reduce uncertainties related to poor estimations of surface area in cells with complex geometries (32) or with membrane corrugations (31), to better control the area of suspended model membranes (36) and to reduce the presence of defects in supported membranes (26). Efforts have also been devoted to increase the spatial resolution of the measuring techniques by resorting to scanning probe microscopic techniques (37). In particular, in recent years, we developed Scanning Dielectric Microscopy (SDM), a scanning probe technique that combines either current-sensing Atomic Force Microscopy (38) or Electrostatic Force Microscopy (39) with analytical or numerical theoretical models (40), (39), (41) to extract the capacitance at the nanoscale. This technique, in force detection mode, has also been demonstrated in the liquid environment (in-liquid SDM) (42), and we previously applied it to the study of thin dielectric films (42) and monocomponent supported lipid bilayers patches (43) in electrolyte solutions.

Here, we exploit the full potential of in-liquid SDM to study the effect of cholesterol on the specific capacitance of supported lipid bilayers patches. With its high spatial resolution, in-liquid SDM has the unique capability to be able to compare *in-situ* the dielectric properties of heterogeneous samples containing bilayer patches with different cholesterol content. To

demonstrate it we considered 1,2-dioleoyl-sn-glycero-3-phosphocholine (DOPC) bilayer patches with and without cholesterol. DOPC is a double unsaturated homoacid phospholipid and is one of the main components of eukaryotic cell membranes. This lipid is in a liquid disordered phase (Ld) at room temperature ( $T_{\text{DOPC}} = -20^{\circ}\text{C}$ ) and is responsible for the fluid nature of cell membranes, a ubiquitous property in signal transduction, transport and cell adaptation.

## RESULTS

In-liquid SDM (see Refs. (42), (43), (44)) uses a metal coated Atomic Force Microscopy probe with a tip with radius in the range  $\sim 10\text{--}100$  nm. Briefly, the sample is scanned by the probe in a two-pass line by line mode: in the first pass the sample surface topography is recorded with no voltage bias applied. In the second pass the tip is lifted at a constant distance with respect to the substrate (larger than the Debye screening length) with an applied amplitude modulated voltage with frequency,  $\omega$ , in the MHz range (beyond the electrolyte dielectric relaxation frequency) and modulation frequency,  $\omega_{\text{mod}}$ , in the kHz range (below the mechanical resonance frequency of the probe), i. e.  $v(t) = v_0/2(1 + \cos(\omega_{\text{mod}}t))\cos(\omega t)$ , where  $v_0$  is the voltage amplitude. This voltage has three harmonics at  $\omega - \omega_{\text{mod}}$ ,  $\omega$  and  $\omega + \omega_{\text{mod}}$ , all of them in the MHz range (44). The low frequency modulation of the signal is just used to increase the signal to noise ratio in the detection. The electric force acting on the probe at such high frequencies depends quadratically on the applied voltage as  $F_{el}(t) = 1/2(dC/dz)v^2(t)$ , where  $dC/dz$  is the system capacitance gradient. Several force harmonics are induced due to this quadratic dependence, of which the one at the modulation frequency, given by  $F_{\omega_{\text{mod}}} = 1/8(dC/dz)v_0^2$ , is measured by means of a lock-in amplifier. From it, local values of the system capacitance gradient,  $dC/dz$ , are obtained. Comparing the measured values of  $dC/dz$  with the theoretical ones obtained by numerically solving Poisson's equation or equivalent models, one extracts the local values of the

specific capacitance of the sample (see Materials and Methods and Refs. (42), (43) for further details). By measuring forces rather than currents, this technique is less affected by stray capacitance effects, and hence has the potential to access specific capacitance values on sub-micrometric areas, and hence to produce high spatial resolution maps of the specific capacitance (45). Moreover, it also offers direct access to the sample thickness, either directly on patch membrane samples or indirectly through force spectroscopy measurements on extended membranes, thus enabling evaluating whether a given change in the specific capacitance is either due to a variation of the thickness or of the dielectric properties of the membrane (or to both).

Figure 1a shows an Atomic Force Microscopy (AFM) topographic image of DOPC bilayer patches supported on a flat gold substrate functionalized with 2-Mercaptoethanol in milliQ water. The bilayer patches have been formed from the deposition of DOPC liposomes (see Materials and Methods). A height profile measured along the dashed line in Fig. 1a is shown in Fig. 1c (black line). The membrane patches along the profile are  $\sim 4.2$  nm thick (see also histogram analysis in Supporting Information S1). This value is in agreement with thickness values reported for solid supported DOPC patches by AFM (46) ( $\sim 4.2$  nm) and quantitative Differential Interference Contrast Microscopy (qDIC) (47) ( $\sim 4.1$  nm), and slightly smaller than the steric thickness measured on unilamellar vesicles by Small Angle Neutron Scattering (SANS) or Small Angle X-Ray Scattering (SAXS) (48), (49) ( $\sim 5$  nm). The lateral sizes of the patches ranges from few micrometres down to  $\sim 200$  nm.

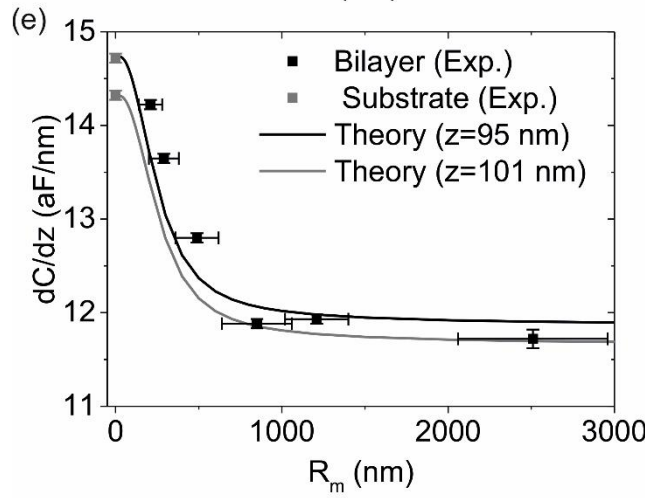
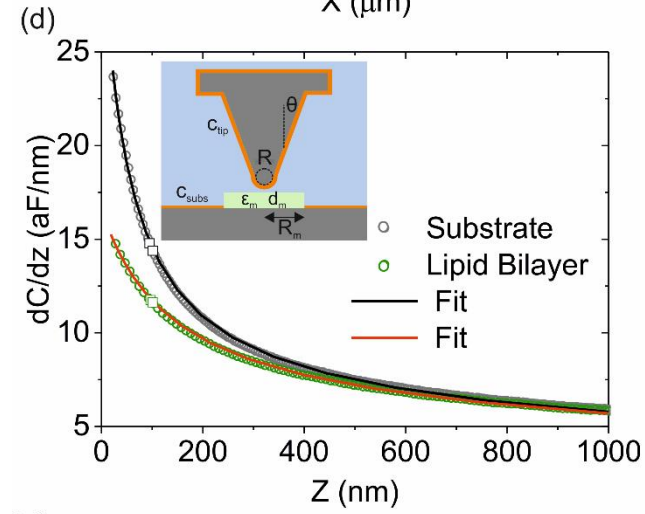
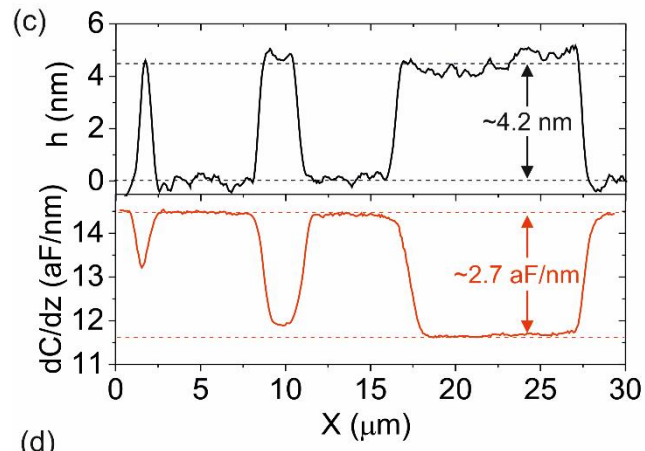
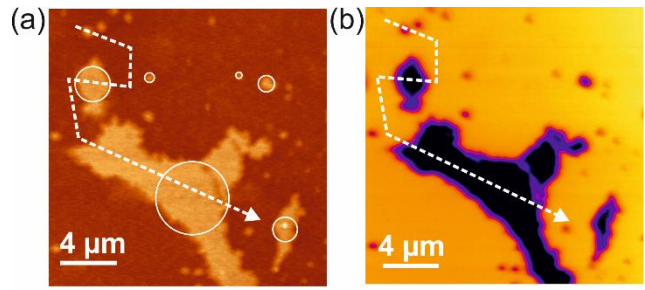


**Figure 1.** (a) AFM topographic and (b) in-liquid SDM dielectric images, respectively, of DOPC bilayer patches on a functionalized planar gold substrate in milliQ water. In-liquid SDM experimental parameters: equivalent spring constant 0.45 N/m, applied voltage amplitude 0.75 V, frequency 5 MHz, modulation frequency 6 kHz, tip-sample distance  $z=101$  nm. (c) Height (black line) and capacitance gradient (red line) profiles along the dashed lines in (a) and (b), respectively. (d) Capacitance gradient approach curves measured on the bare substrate (grey circles) and on the centre of the largest DOPC patch (olive circles). Continuous lines represent a least square fitting of theoretical curves calculated with the model shown in the inset to the experimental data. The extracted parameters are listed in Table 1. The black and olive square symbols correspond to the capacitance gradient values on the substrate and centre of the largest DOPC bilayer patch in (b), respectively, from where the tip sample distance is obtained. (e) (black symbols) Capacitance gradient values measured on the centre of the DOPC bilayer patches in (a) as a function of the effective patch radius (defined from the circles in (a)). The grey symbols represent representative values on the substrate. (continuous lines) Theoretical dependence of the capacitance gradient as a function of the radius of the DOPC bilayer patch obtained with the model in the inset in (d). The parameters used in the calculations are those obtained from (d) and listed in Table 1 for DOPC.

Figure 1b shows an in-liquid SDM image of this sample obtained at 5 MHz in constant height mode at a height  $z=101$  nm (see Materials and Methods for details and Supporting Information S2 for additional images at different tip-substrate distances). It shows variations of the electric force, represented here through the capacitance gradient,  $dC/dz$  (see above, Refs. (39), (42) and Materials and Methods). The in-liquid SDM image reveals the presence of the DOPC bilayer patches down to lateral sizes  $\sim 200$  nm. The contrast in the SDM image shows an excellent

signal-to-noise ratio (up to  $\sim 2.7$  aF/nm signal for a noise floor of  $\sim 0.05$  aF/nm, see capacitance gradient cross section profile in Fig. 1c, red line). This excellent contrast has been achieved by enlarging on purpose the tip radius by scratching the tip on a bare clean substrate prior to its use. The contrast in the SDM image is negative indicating that the dielectric constant of the bilayer patches is smaller than that of the electrolyte solution surrounding them, similarly to what observed earlier for DPPC bilayer patches on highly doped silicon substrates (43).

The quantitative extraction of the specific capacitance of the bilayer patches has been done by measuring cantilever oscillation amplitude at the  $\omega_{\text{mod}}$  harmonic versus distance curves and deriving from it capacitance gradient,  $dC/dz$ , versus distance curves (referred on what follows as capacitance gradient approach curves, see Materials and Methods) on the bare substrate and on the centre of the largest membrane patch (grey and olive circles in Fig. 1d, respectively), and by fitting to them theoretical capacitance gradient approach curves numerically calculated with the model in the inset of Fig. 1d, following procedures developed in previous works (see Materials and Methods). Here, in the model we included an interfacial capacitance to the tip,  $c_{\text{tip}}$ , necessary when dealing with metallic substrates to account for the adsorption of ions, the reduced dielectric constant of interfacial water (50) and other interfacial effects (see Materials and Methods for further details). The fitted curves are shown by continuous lines in Fig. 1d, and the parameters extracted are summarized in Table 1 for two characteristic values of the tip interfacial capacitance, namely,  $c_{\text{tip}}=2 \mu\text{F}/\text{cm}^2$  and  $4 \mu\text{F}/\text{cm}^2$  (45). The fittings have been made down to distances  $\sim 20$  nm. Below this distance other interactions due to van der Waals forces or the presence of diffusive space charge layers may enter into play, which are not included in the theoretical model. The agreement between the theoretical and the experimental curves is excellent. The specific capacitance of the DOPC bilayer patch obtained is  $c_{\text{DOPC}}\sim 0.7\text{--}0.8$

$\mu\text{F}/\text{cm}^2$ , which is in reasonable agreement with values reported for similar lipid bilayers measured free from solvent contributions by means of macroscopic techniques (28). We remark that while the interfacial capacitance of the substrate depends strongly on the chosen tip interfacial capacitance (45), the specific capacitance of the lipid bilayer is almost insensitive to it.

**Table 1.** Specific capacitance of the lipid bilayer patches obtained from the analysis of the experimental data in Figs. 1d and 2d. The parameters of the tip geometry and substrate obtained from the same analysis are also shown. Parameters without errors are fixed.

$C_{\text{tip}}$ $\mu\text{F}/\text{cm}^2$	$C_{\text{DOPC}}$ $\mu\text{F}/\text{cm}^2$	$C_{\text{DOPC:chol}}$ $\mu\text{F}/\text{cm}^2$	$C_{\text{sub}}$ $\mu\text{F}/\text{cm}^2$	R nm	$C'_{\text{off}}$ aF/nm	$\theta$ deg
DOPC						
2	$0.8 \pm 0.1$	-	$3.1 \pm 0.1$	$370 \pm 25$	$0.78 \pm 0.05$	21
4	$0.7 \pm 0.1$	-	$1.9 \pm 0.1$	$351 \pm 25$	$0.71 \pm 0.05$	21
DOPC and DOPC:chol						
2	$1.0 \pm 0.1$	$0.7 \pm 0.1$	$2.1 \pm 0.1$	$310 \pm 25$	$1.10 \pm 0.05$	21
4	$0.9 \pm 0.1$	$0.6 \pm 0.1$	$1.5 \pm 0.1$	$287 \pm 25$	$1.06 \pm 0.05$	21

We note a feature that was also observed in Ref. (45), namely, that the capacitance gradient (force) contrast in Fig. 1b shows a remarkable dependence on the lateral size of the membrane patches (see also cross-section profile in Fig. 1c, red line). This dependence is illustrated in Fig. 1e where we plot the capacitance gradient values on the centre of each DOPC bilayer patch as a function of the patch equivalent radius,  $R_m$  (symbols). The equivalent radius has been estimated from circles centred on the patches as shown in Fig. 1a (for the uncertainty in the radii see Supporting Information S3). For reference, we also plotted in Fig. 1e characteristic values of the

capacitance gradient on the substrate (grey symbols in Fig. 1e). Two factors can induce a dependence of the capacitance gradient on the lateral size of the patches, namely a finite-size electrostatic effect related to the relative size of the patch with respect to the scanning probe tip and a variation of the specific capacitance of the patches with their width. To answer this question, we have calculated the theoretical expected variation of the capacitance gradient as a function of the the radius of the DOPC bilayer patch by using the model shown in the inset of Fig. 1d. In the simulations we used the parameters derived from the quantitative analysis performed on the largest patch (Table 1), with no further free parameter. The results are shown in Fig. 1e (continuous lines) for two tip-substrate distances compatible with the measurements,  $z=95$  nm and  $z=101$  nm (the different distances account for the slight tilting of the image and the fact that the static bending of the cantilever when the tip is on top of the largest patch is smaller than when on the smaller patches or the substrate). The numerical calculations nicely follow the experimental trend, within the uncertainty of the experiments. We therefore conclude that down to the smallest patches detected ( $\sim 200$  nm), the specific capacitance of DOPC bilayer patches does not depend on its lateral size, although the measured capacitance gradient strongly depends on it. For DOPC bilayer patches larger than a few micrometres the force becomes independent from the lateral size of the patches (see Fig. 1e), and it can be directly correlated to the membrane specific capacitance (a larger force directly indicates a smaller specific capacitance). Otherwise, lateral finite size effects, which originates in the tip-sample electrostatic interaction, should be considered. Remarkably lateral finite-size effects in in-liquid SDM (45) are much larger (micrometres) than those found in air (41) due to the stronger contribution of the cone part of the tip.

We analyse now the effect of cholesterol on the specific capacitance of the supported DOPC bilayer patches. We prepared a sample containing both DOPC and DOPC:chol bilayer patches by successive depositions of the corresponding liposomes (see Materials and Methods). Figure 2a shows a topographic AFM image of the sample (see Supporting Information S3 for a larger area image). A height profile measured along the dashed line in Fig. 2a is shown in Fig. 2c (black line). In it two groups of membrane patches with slightly different thicknesses,  $\sim 3.2$  nm and  $\sim 3.7$  nm are observed (see also histogram analysis in Supporting Information S1). The presence of patches with two different thicknesses agrees with the sample being prepared from liposomes with and without cholesterol, and with the fact that cholesterol is known to thicken DOPC bilayers (48), (49), (51), (52), (53). Here, we observe a thickening of around  $\sim 16\%$  (Fig. 1c, black line), which is in reasonable agreement with the thickening predicted for DOPC bilayers at 40%-50% cholesterol content ( $\sim 13\%$ – $19\%$ ) (48), (49), (53). The thicker membrane patches are, then, expected to be composed of DOPC:chol (see further confirmation below). We note that the absolute value of the thickness of the DOPC patches in Fig. 2 is somewhat smaller ( $\sim 1$  nm) than the one reported in Fig. 1. We attribute it to the fact that the imaging acquisition settings for mixed samples were different from those of pure samples and that they have been selected to optimize the electrical images. Therefore, the height values in these images could be somewhat underestimated, although the relative height difference between DOPC and DOPC:chol patches seems to be correct. The widths of both types of patches span again a range from  $\sim 200$  nm up to few micrometres.

Figure 2b shows a constant height in-liquid SDM image of the sample in Fig. 2a acquired at 5 MHz and  $z=93$  nm (see Supporting Information S2 for additional images at different tip-substrate distances). The dielectric contrast is again negative for all patches, and patches down to  $\sim 200$  nm

can be electrically detected. The more relevant feature displayed in Fig. 2b is the large difference (~79 %) in the dielectric contrast observed between the two largest patches in the image (see capacitance gradient profile in Fig. 2c, red line). This large contrast variation should be compared with the small relative variation in thickness (~16%, see Fig. 2c, black line). Therefore, it cannot be fully attributed to the thickening effect. It cannot be attributed neither to a difference in the lateral size of the patches, since both patches are few-micrometre large and, hence, their capacitive signals are independent from the lateral size of the patches, as discussed above. Therefore, the large difference in the dielectric contrast must reflect a variation in the dielectric properties of the DOPC lipid bilayer due to the presence of cholesterol.

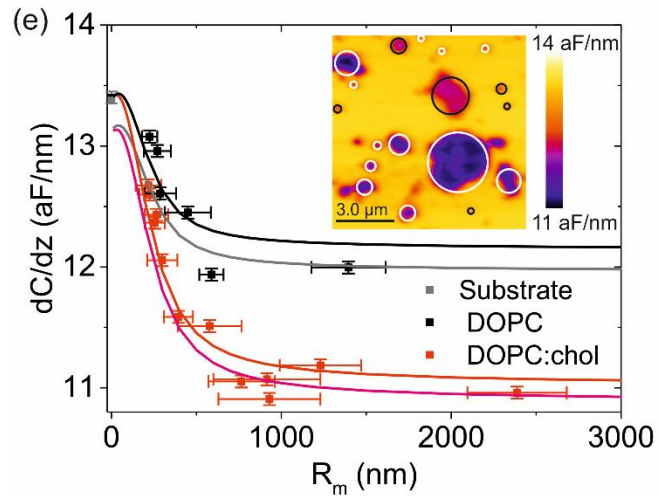
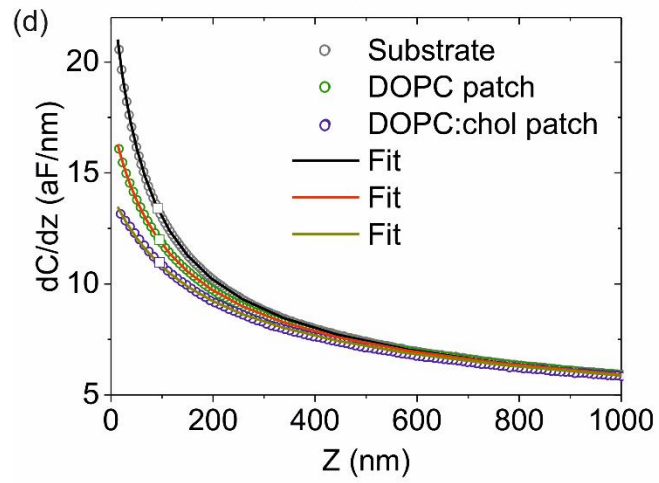
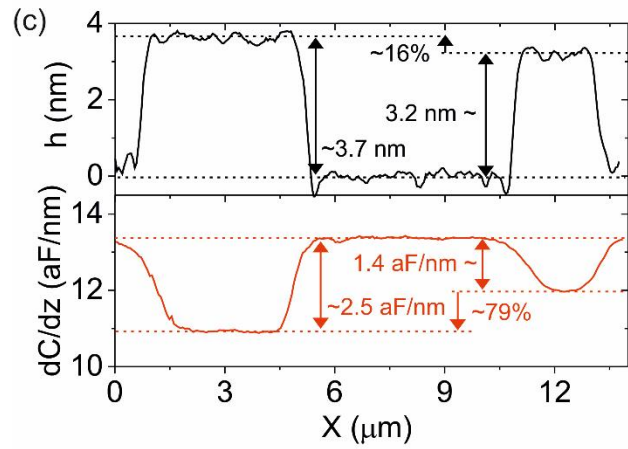
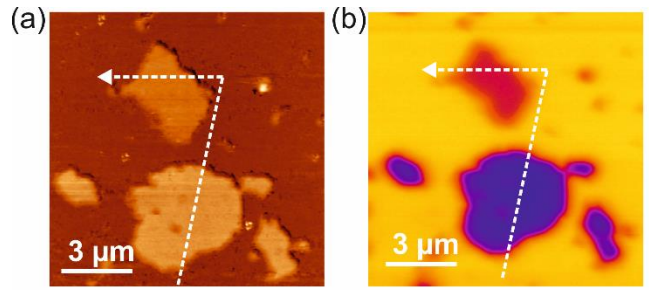


**Figure 2.** (a) AFM topographic and (b) SDM images of a sample containing DOPC and DOPC:chol bilayer patches in a 1 to 1 proportion supported on a functionalized planar gold substrate in milliQ water. SDM experimental parameters: equivalent spring constant 0.45 N/m, applied voltage 0.75 V, frequency 5 MHz, modulation frequency 6 kHz, tip-sample distance  $z=93$  nm. (c) Thickness (black line) and capacitance gradient (red line) profiles along the dashed lines in (a) and (b), respectively. (d) Capacitance gradient approach curves measured on the bare substrate (grey symbols) and on the two largest patches in (b) (olive and violet symbols, respectively). Continuous lines represent least square fitting of theoretical data generated with the model in the inset in Fig. 1d. Extracted parameters are shown in Table 1. The grey, olive and blue square symbols correspond to the values of the capacitance gradient on the substrate and the two largest membrane patches of the SDM image in (b), from where the tip sample distance is obtained. (e) (symbols) Capacitance gradient values on the centre of the DOPC bilayer patches highlighted in the large area in-liquid SDM image in the inset as a function of the effective radius of the patches. Symbols of the same colour correspond to patches with similar thickness. (continuous lines) Theoretical dependence of the capacitance gradient as a function of the radius of the DOPC bilayer patch obtained from the model in the inset in Fig. 1d. The parameters used in the calculations are those obtained in (d) and listed in Table 1 (DOPC and DOPC:chol). The black and red lines correspond to tip sample distances  $z=91$  nm, while the grey and pink lines to  $z=95$  nm, compatible with the measurements.

To investigate this effect, we have quantified the specific capacitances of the two largest lipid bilayer patches in Fig. 2a by acquiring capacitance gradient approach curves on their centres and on the bare substrate by proceeding as described above (Fig. 2d). The parameters obtained from

this analysis are shown in Table 1. The relative difference between the specific capacitance of the DOPC bilayer patches without and with cholesterol ( $c_{\text{DOPC}} \sim 0.9 \mu\text{F}/\text{cm}^2$  and  $c_{\text{DOPC:chol}} \sim 0.6 \mu\text{F}/\text{cm}^2$ , respectively) is  $\sim 35\%$ , much larger than the observed thickness variation ( $\sim 16\%$ ), thus confirming that cholesterol reduces the dielectric response of the DOPC bilayer patches (see discussion section).

The conclusions reached for the two largest patches in Fig. 2a are confirmed for the sub-micrometric lipid bilayer patches present in the sample. Figure 2e shows the capacitance gradient measured at the centre of patches in the figure in the inset of Fig. 2e, which is a zoom out of Fig. 2b (a similar analysis for a larger area image is provided in the Supporting Information S4). Patches ranging from  $\sim 200$  nm up to several micrometres are considered. The thinner patches (DOPC) are represented by the black symbols and surrounded with a white circle in the inset of Fig. 2e, while the thicker ones (DOPC:chol) are represented by the red symbols and surrounded by a black circle. Two distinct dependencies are clearly observed for the two groups of patches. Finite element numerical calculations (continuous lines in Fig. 2e) show that each group of patches can be described by a single specific capacitance, corresponding to the values reported in Table 1. These results confirm that down to  $\sim 200$  nm the lateral size does not affect the value of the specific capacitance of the DOPC:chol bilayer patches, like we showed above and here again for DOPC bilayer patches, and that the thicker patches (DOPC:chol) show a much lower specific capacitance than thinner ones (DOPC).

To further confirm that thicker bilayer patches correspond to those containing cholesterol, we have considered an additional sample prepared by reducing by a factor of three the concentration of DOPC:chol liposomes in the solution (so that we expect DOPC:chol bilayer patches to be much less abundant than DOPC ones). Figures 3a and 3b show, respectively, large area AFM

topographic and in-liquid SDM images obtained on this sample. In the topographic image (Fig. 3a) two groups of patches with different thicknesses can be identified from a careful analysis (see Supporting Information S5). We marked with white and black circles the thin and thick patches, respectively (only supra-micrometric patches have been analyzed). Thicker patches are clearly much less abundant, what by taking into account the sample composition, confirms that they correspond to DOCP:chol.

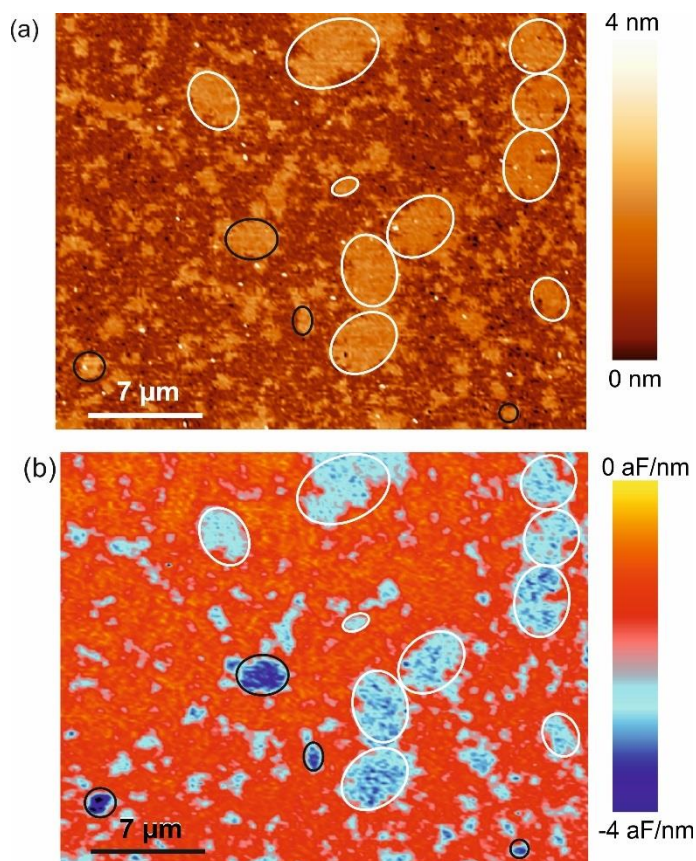


**Figure 3.** (a) AFM topographic and (b) in-liquid SDM dielectric images of a sample containing DOPC and DOPC:chol membrane patches in a 3:1 proportion on a functionalized planar gold substrate in milliQ water. SDM experimental parameters: equivalent spring constant 0.76 N/m, applied voltage 0.75 V, frequency 5 MHz, modulation frequency 6 kHz and tip-sample distance  $z=11$  nm. In (a) and (b) black and white circles identify thicker and thinner patches with supra-

micrometric sizes ( $>1 \mu\text{m}$ ), respectively. The colour scale is different from that of Figs. 1 and 2 and it has been chosen to highlight the difference in contrast between the two type of patches for this sample.

The in-liquid SDM image (Figs. 3b) shows also two distinct contrasts for the patches analyzed. The thicker patches (black circles corresponding to DOCP:chol) show larger contrasts, indicating that they have a smaller specific capacitance (remember that for large patches the SDM contrast can be correlated directly to the specific capacitance of the patch). These results then unambiguously confirm that DOPC:chol bilayer patches show a strong reduction of the specific capacitance as compared to pure DOPC bilayer patches.

## DISCUSSION

We have found that cholesterol at a 50% concentration largely reduces (by an amount  $\sim 35\%$ ) the specific capacitance of DOPC bilayer patches. This reduction cannot be attributed to the slight increase in the bilayer thickness ( $\sim 16\%$ ). According to the simple expression for the specific capacitance,  $c_m = \epsilon_0 \epsilon_r / d_m$ , the relative variation in specific capacitance due to both thickness and dielectric constant variations is given by  $\Delta c_m / c_m = \Delta \epsilon_r / \epsilon_r - \Delta h / h$ . Since the thickness variation amounts to only  $\Delta h / h \sim 16\%$ , the remaining variation should correspond to a *decrease* of the dielectric constant of the lipid bilayer caused by the presence of cholesterol,  $\Delta \epsilon_r / \epsilon_r \sim -20\%$ . A possible explanation of the reduction in the dielectric constant observed can be attributed to a reduction of the hydration level of the DOPC bilayers containing cholesterol. To support this statement we calculate the dielectric constants of the DOPC and DOPC:chol patches and compare them with the corresponding values obtained earlier in air environment by using the same technique (54). By taking the measured bilayer thickness from Fig. 2 ( $d_{DOPC} \sim 3.2 \text{ nm}$ ) and

the measured specific capacitance ( $c_{DOPC} \sim 0.9 \mu\text{F}/\text{cm}^2$ ), the dielectric constant of pure DOPC bilayers in milliQ water is  $\epsilon_{DOPC,liq} \sim 3.2$  (a similar value is also obtained from the measurement in Fig. 1, in which the thickness was  $\sim 4.5 \text{ nm}$  and the specific capacitance  $\sim 0.7 \mu\text{F}/\text{cm}^2$ ). This value matches the one we obtained earlier with the same technique on DPPC bilayer patches in liquid,  $\epsilon_{DPPC,liq} \sim 3.2$  (43), and is larger than the value  $\epsilon_{DOPC,dry} \sim 2$  measured in dry air conditions (54). The larger dielectric constant observed in liquid environment was attributed to the hydration of the polar head groups of the lipid bilayers (43). For the DOPC:chol patches, instead, by using a thickness  $d_{DOPC:chol} \sim 3.7 \text{ nm}$  and a specific capacitance  $c_{DOPC:chol} \sim 0.6 \mu\text{F}/\text{cm}^2$ , the dielectric constant obtained in liquid is  $\epsilon_{DPPC:chol,liq} \sim 2.5$ . This value is similar to the values obtained for DOPC bilayer patches and cholesterol crystals in dry conditions ( $\epsilon_{DOPC,dry} \sim 2$  and  $\epsilon_{chol,dry} \sim 2.3$ ) (54). This result suggests that at 50% chol content DOPC:chol patches are hardly hydrated, contrary to what happens with pure DOPC patches. The reorganization of the head groups in the presence of cholesterol necessary to achieve a non-hydrated configuration is the same than the one assumed in the so-called umbrella model, used to explain the solubility of cholesterol in lipid bilayers (55) and other properties (20).

On the other hand, we note that the specific capacitances of DOPC bilayer patches reported here, and their variation with cholesterol, are in striking agreement with recent results reported for supported DMPC+DMTAP bilayers with and without cholesterol and obtained from macroscopic electrochemical impedance spectroscopy (26) with strict control of bilayer quality (e.g. absence of bilayer defects and of solvent).

The use of in-liquid SDM in force detection mode has shown relevant advantages in the present study as compared to current/voltage time varying macroscopic techniques (22). First, in-liquid SDM displays a high spatial resolution (45), what enables studying isolated lipid bilayer

patches, with no need to consider extended defect-free lipid bilayers, required for macroscopic measurements. Second, it enables comparing directly the specific capacitances of different bilayer patches with different composition *in situ* and under the same experimental conditions, reducing uncertainties related to successive independent measurements. In-liquid SDM also provides direct access to the bilayer thickness, thus enabling identifying whether a specific capacitance variation is associated with either a thickness or a dielectric constant variation. Finally, in-liquid SDM measurements are performed at high frequencies in the MHz range (beyond the dielectric relaxation frequency of the electrolyte solution). In this frequency range, the capacitance contribution associated to ionic diffusive space charges can be neglected (45), what simplifies the quantitative analysis. For measurements performed at lower frequencies (e.g. below kHz, as in the case of most existing macroscopic techniques (28)), the diffusive space charge capacitance needs to be accounted for and subtracted from the measurements, which is not always simple and can introduce some inaccuracy and variability in the values thus obtained, depending on the assumptions made.

Concerning the accuracy of the specific capacitance values obtained for supported lipid bilayers by in-liquid SDM some considerations are in order. The electric force measured by the in-liquid SDM probe depends on the whole system capacitance gradient, which includes contributions from the tip-electrolyte interface, the electrolyte, the electrolyte-membrane-substrate interface, and the electrolyte-substrate interface. The bulk electrolyte contribution is accounted for by solving the Poisson's equation for the tip-sample system with realistic and calibrated tip and sample geometries. The tip-electrolyte interfacial contribution at the frequencies of the measurements (MHz) is expected to include only effects from the so-called compact or Stern layer,  $C_{tip}=C_{int,tip}$  (45). The substrate-electrolyte interface, instead, includes

contributions from both the functionalization self-assembled monolayer,  $c_{SAM}$ , and its interface with the electrolyte,  $c_{int,SAM}$ , i.e.  $c_{sub}=(c_{SAM}^{-1}+c_{int,SAM}^{-1})^{-1}$ . Finally, the electrolyte-membrane-substrate interface includes contributions from the self-assembled monolayer on the substrate,  $c_{SAM}$ , the lipid bilayer itself,  $c_m^*$ , and the interfacial lipid bilayer-electrolyte compact layer,  $c_{int,m}$ , i.e.  $c_m=(c_{SAM}^{-1}+c_{int,m}^{-1}+c_m^{*-1})^{-1}$ . Since the functionalization SAM used here is very short (two carbons) and the compact layer is usually also very short (a few water layers) we expect that their respective specific capacitances will be much larger than the specific capacitance of the lipid bilayer, so that the measured values,  $c_m$ , are expected to be good estimations of the lipid bilayer specific capacitance,  $c_m^*$  ( $c_m \sim c_m^*$ ). Finally, we note that the uncertainty in the value of the tip interfacial capacitance,  $c_{tip}$ , ( $c_{tip}=2-4 \mu\text{F}/\text{cm}^2$ , (45)), introduces a minor uncertainty on the specific capacitance values of the lipid bilayer patches,  $c_m$ , as it can be seen in Table 1. The uncertainty is larger for the value of  $c_{sub}$  since it is of the same order of magnitude than  $c_{tip}$ , as discussed elsewhere (45). Other substrate effects such roughness (rms~0.2-0.3 nm in the present study) or a reduction of the lipid lateral mobility (which involve diffusion times much longer than the period of the ac voltage) are not expected to affect the extracted values of the bilayer specific capacitances.

In the present work we have compared the specific capacitance of mixed samples containing pure DOPC and DOPC:chol bilayer patches at a fairly large cholesterol concentration (50%), close to the cholesterol solubility limit. The relative variation measured (~35%) is expected to be close to the maximal relative variation that can be found with solubilized cholesterol. For smaller cholesterol concentrations a smaller relative variation of the specific capacitance is expected according to the monotonous trend with cholesterol concentration shown by other physical properties (e.g. thickness, bending rigidity or area per lipid) in DOPC bilayers (49), (53).

Preparing mixed samples containing patches with several intermediate cholesterol concentration by the successive liposome deposition method used here has been found challenging, and further research to find alternative sample preparation methods becomes necessary to explore simultaneously several intermediate cholesterol concentrations by SDM.

The results presented in this work open interesting applications in the analysis of natural membranes, which are highly heterogeneous composition and structure (56), (57), as well as, to address the electrical properties of small scale biomembrane structures such as exosomes (58), outer membrane vesicles (59) or membrane nanoextensions, some of which show especial electric properties (60).

## CONCLUSIONS

We have shown by means of in-liquid Scanning Dielectric Microscopy in force detection mode that cholesterol at 50% concentration strongly reduces the specific capacitance of supported DOPC bilayer patches. The reduction observed (~35%) is partially due to a small increase in the membrane thickness (~16%), but, overall, to a significant reduction in the dielectric constant of the lipid bilayer itself (~20%). The reduction of the dielectric constant of the DOPC:chol bilayer patches could be associated to the dehydration of the polar head groups caused by the presence of cholesterol molecules. This conclusion has been observed to hold for lipid bilayer patches down to, at least, ~200 nm in lateral size. The results presented here have confirmed the potential of in-liquid SDM to measure the specific capacitance of artificial and natural biomembranes at high spatial resolution with important implications in biology, biochemistry or biosensor characterization.

## MATERIALS AND METHODS

**Metallic substrates.** We used flat gold substrates produced by the mica replica method (MicroFab Space, IBEC), functionalized with self-assembled monolayers (SAMs) made of 2-Mercaptoethanol 99.0% (Sigma-Aldrich). The SAMs were prepared by incubation of the gold substrates in a 1 mM solution of the thiols overnight at 2–8°C, protecting the vial from light, and from oxidation by a nitrogen flow. Gold was selected for its excellent conductive properties, while the alcoholic moiety terminating the thiol molecules was selected to make the surface more hydrophilic, promoting the interaction with the lipid polar heads and the formation of intact bilayers from liposomes.

**Lipid bilayer patches samples.** DOPC (1,2-dioleoyl-sn-glycero-3-phosphocholine) and DOPC:chol (50% concentration) bilayer patches were formed on the gold functionalized substrates by the liposome fusion method. For the preparation of the liposomes chloroform and methanol, HPLC grade, were purchased from Sigma Aldrich; high purity water (18.2 MU cm) was obtained with a MilliQ water purification system (Millipore); DOPC specified as R99% pure, was obtained in powder form (Avanti Polar Lipids, Merk) and used without further purification. The DOPC liposomes were prepared as follows: DOPC was first dissolved in chloroform/methanol (3:1) (v/v) solution to a final lipid concentration of 10 mM. Then the solvent was evaporated under a nitrogen stream with constant rotation of the vial. The vial was kept in vacuum for 6–8 hours to ensure the absence of organic solvent traces. The dry lipid was then resuspended in distilled water at ~60°C to its final concentration of 0.1 mM. The liposomes were spontaneously formed under these conditions and stored at 2°C –8°C, always protected from light, and used within 1–2 days. The DOPC:chol liposomes were prepared in a similar way. Cholesterol was dissolved in chloroform at a concentration of 10 mM. 5  $\mu$ L of DOPC stock

solution and 5  $\mu\text{L}$  of chol stock solution, both 10 mM, were then mixed in a vial and sonicated in ice for 5-10 minutes to ensure disintegration of possible cholesterol aggregates, homogenization of the components and inclusion of cholesterol in the lipid bilayer (chol is expected to completely dissolve in fluid-like liquid disordered (Ld) lipid bilayers like DOPC ones). The solvent was evaporated as previously detailed and the 'lipid film-cake' was rehydrated with 1 mL of milliQ at about 60°, to a final lipid concentration of 0.1 mM. The liposomes formed were stored at 2-8°C, protected from light and used within 1-2 days. For the monocomponent DOPC sample, a drop of 80  $\mu\text{L}$  of the DOPC liposome suspension was added to the gold substrate at room temperature (25°C) and incubated for 30 min at 60°C. The concentration, temperature and deposition time were selected to ensure the formation of lipid bilayers only partially covering the surface (bilayer patches). Afterwards, the substrate was rinsed several times with water to remove the excess of vesicles in suspension. For the mixture sample containing DOPC and DOPC:chol bilayer patches, first 40  $\mu\text{L}$  of pure DOPC liposome solution and then 40  $\mu\text{L}$  of DOPC:chol 1:1 liposome solution were subsequently added to the substrate with an intermediate rinsing step to remove any non adhered DOPC liposome. This sample preparation procedure was used to prevent mixing/fusion of liposomes of different types. The reduced lipid mobility on the functionalized gold substrate and the selected deposition conditions lead to the formation of isolated lipid bilayer patches of the two components (otherwise a homogeneous DOPC:chol bilayer would be formed). Four different samples have been analysed in the present study containing respectively DOPC patches, DOPC:chol patches (data not shown), DOPC and DOPC:chol patches (1/1) and DOPC and DOPC:chol patches (3/1).

**In-liquid SDM measurements.** In-liquid SDM measurements were done by following the methodology described in Ref. (42), by using an amplitude modulated ac voltage

$v(t) = v_0/2(1 + \cos(\omega_{\text{mod}}t))\cos(\omega t)$  applied between a conductive AFM cantilever probe and the gold substrate in liquid in a Cervantes commercial AFM system (Nanotec Electronica S.L.). The applied voltage had amplitude 0.75 V, electrical frequency 5 MHz and modulation frequency 6 kHz, and was applied with an external waveform generator (model No. 33250A, Agilent Technologies) combined with an external lock-in (LockIn 204/2, Anfatec Instruments). The low frequency value ( $\sim 6$  kHz) was chosen to be well below the resonance frequency of the probes in liquid ( $\sim 35$  kHz). The high frequency value ( $\sim 5$  MHz) was chosen to be larger than the dielectric relaxation frequency of the electrolyte in the drop used to perform the experiments (estimated to be in the hundreds kHz's) and to provide the best signal to noise ratio (in the MHz range the frequency response of the external electrical circuit can affect the signal reaching the tip-sample gap). The applied potential induces an oscillating electrical force acting on the tip which contains several harmonics. The oscillation amplitude at the  $\omega_{\text{mod}}$  frequency,  $A_{\omega_{\text{mod}}}$ , was measured with the lock-in amplifier. The measured oscillation amplitude was converted to capacitance gradient values through the relationship (45)  $dC/dz = \alpha 8k(A_{\omega_{\text{mod}}} - A_{\omega_{\text{mod}},\text{off}}) / v_0^2 m$  where  $A_{\omega_{\text{mod}},\text{off}}$  is the lock-in offset,  $k$  the spring constant,  $m$  the photodiode sensitivity and  $\alpha$  a renormalization factor close to 1, which accounts for the potential losses in the electric circuitry due to the use of frequencies in the MHz range and to inaccuracies in the determination of the photodiode sensitivity and spring constant (45). Raw data corresponding to the  $dC/dz$  curves reported in the manuscript are shown in the Supporting Information S6. We used HQ:NSC19/Cr-Au gold coated AFM probes (MikroMash) with a spring constant in the range 0.05 – 2.3 N/m, calibrated using Sader's method. Topographic and  $dC/dz$  images were acquired in the two pass mode line by line, with the topography being recorded in conventional intermittent contact mode (with no potential applied) and the  $dC/dz$  image in constant height mode in off-feedback with the potential applied

and with no mechanical oscillation applied. The tip-substrate distance in the electrical images was set larger than  $\sim 100$  nm to ensure non-contact with the sample and to be safely larger than both the Debye screening length and the range of the van der Waals interaction, which were estimated to be at most  $\sim 20$  nm from the approach curves. The image acquisition settings (set point, scan speed and gains) were chosen to optimize the electrical images rather than the topographic images, which in some cases produced topographic images with underestimated thicknesses. As in previous works (38), (39), (42), (43), (61) approach curves ( $N=10$ ) were measured on selected positions of the sample (typically on the bare substrate and on the centre of large membranes patches) to calibrate the tip geometry, determine the SDM imaging distances, the lipid bilayer specific capacitances and the substrate and tip interfacial capacitances. The approach speed of the approach curves was typically  $\sim 300$  nm/sec. For each sample a large area image was first acquired, followed by one or two successive zoom-ins until the desired areas were identified. In these areas, electrical images at three different tip-substrate distances were acquired. Further imaging was prevented by tip contamination, probably enhanced by the applied electric potential.

**Finite element numerical calculations.** We quantitatively analysed the  $dC/dz$  curves following the methodology applied in Refs. (39), (43), and earlier works, by solving the currents model implemented in the AC/DC Electrostatic module of COMSOL Multiphysics (Comsol Inc.). For frequencies beyond the dielectric relaxation frequency of the electrolyte, this model is equivalent to a quasi-static dielectric model (Poisson's model), and it correctly describes in-liquid SDM measurements (45), (62). The probe was modelled as in previous works (39), (61), with the difference that an interfacial capacitance that takes into account ion adsorption, the reduced dielectric constant of water near a surface (50) and other interfacial effects was added to it as

schematically shown in the inset of Fig. 1d (45). Briefly, the tip consists of a conical tip of height  $H$  and half cone angle  $\theta$  ended with a tangent sphere of radius  $R$ . The indirect cantilever contribution was included by adding a disc of thickness  $W$  and radius  $H.\tan(\theta)+L$ , sitting on top of the cone as discussed in Ref. (63). The interfacial capacitance around the tip was modelled by a physical dielectric layer of thickness  $d_{tip}$  and dielectric constant  $\varepsilon_{tip}$  ( $c_{tip}=\varepsilon_0\varepsilon_{tip}/d_{tip}$ ). The use of a physical dielectric layer for the tip, rather than a distributed capacitance (42), (43), facilitates the integration of the Maxwell stress tensor to calculate the force, as discussed elsewhere (45). In most calculations we kept fixed  $d_{tip}=2$  nm and only varied  $\varepsilon_{tip}$ . The lipid bilayer patches were modelled as a dielectric disc of radius  $R_m$ , thickness  $d_m$  and dielectric constant  $\varepsilon_m$  (corresponding to a specific capacitance  $c_m=\varepsilon_0\varepsilon_m/d_m$ ). To represent the functionalized electrode interface, a distributed capacitance,  $c_{sub}$ , was assumed on the substrate (43). For the thicknesses of the lipid bilayers, the electric force acting on the tip only depends on their specific capacitance (see Supporting Information S7). The electric force acting on the probe was determined by integration of the Maxwell stress tensor over the conical part of the tip (integration on the cantilever was avoided to reduce the numerical noise). Direct cantilever effects were modelled phenomenologically through a constant offset,  $C'_{off}$  (45). Capacitance gradient approach curves were calculated by varying the tip-bilayer patch distance in the geometrical model, while capacitance gradient lateral membrane size dependent curves were obtained by keeping the distance fixed and varying the radius of the lipid bilayer patch.

**Extraction of the specific capacitance of the lipid bilayer patches.** To extract the specific capacitance of the lipid bilayer patches we followed a similar approach to the one detailed in Ref. (43), with the modifications discussed elsewhere (45). Since no analytical theoretical expression can be used for the given tip-sample geometry, the approach consists in computing

numerically theoretical  $dC/dz$  vs distance curves, which after interpolation, are fitted to the experimental  $dC/dz$  vs distance curves. We calibrated the tip geometry using  $dC/dz$  curves on the metallic substrate, as in previous works (39), (61), (63). Here, the fittings were done by keeping the half cone angle, cone height and cantilever thickness fixed to manufacturer values ( $H=12.5$   $\mu\text{m}$ ,  $W=3$   $\mu\text{m}$ ,  $\theta=21^\circ$ ) and fixing the tip interfacial capacitance within the range  $c_{tip}\sim 2-4$   $\mu\text{F}/\text{cm}^2$  (45). The voltage reduction factor,  $\alpha$ , was fixed from the long-range part of the  $dC/dz$  curve to give the set half cone angle (45). Their values were very close to one  $\alpha=1-1.02$ . The cantilever length was kept to  $L=3$   $\mu\text{m}$ , which is a reasonable value to include indirect effects with a disc cantilever model (63). The result of the fitting process provided the tip radius,  $R$ , the substrate interfacial capacitance,  $c_{sub}$  and the capacitance gradient offset,  $C'_{off}$ . With the obtained parameters, we calculated capacitance gradient approach curves on the lipid bilayer patch with radius,  $R_m$ , and thickness,  $d_m$ , and fitted them to the experimental approach curve measured on the centre of the lipid bilayer patches, with the dielectric constant of the membrane,  $\epsilon_m$ , as the single fitting parameter. As mentioned above, for the lipid bilayer thicknesses ( $< 10$  nm) the fittings were sensitive to only the lipid bilayer specific capacitance,  $c_m$ , which is the value we reported. The analysis was done with a custom-made software written in Matlab (Mathworks inc.) linked to the COMSOL Multiphysics software.

## ASSOCIATED CONTENT

**Supporting Information.** Histogram Analysis of bilayer thickness of Figs. 1 and 2. Additional SDM images for Figs. 1 and 2 at different tip sample distances. Equivalent bilayer patch radius and uncertainty. Additional data for Fig. 2. Additional data for Figure 3. Raw data for the

capacitance gradient approach curves of Figs. 1 and 2. Dependence of force on the lipid bilayer patch specific capacitance.

## AUTHOR INFORMATION

### **Corresponding Author**

\*ggomila@ibecbarcelona.eu

### **Author Contributions**

The manuscript was written through contributions of all authors. All authors have given approval to the final version of the manuscript.

## ACKNOWLEDGMENT

This work was partially supported by the Spanish Ministerio de Economía, Industria y Competitividad and EU FEDER through Grant No. TEC2016-79156-P and the Generalitat de Catalunya through Grant No. 2017-SGR1079 and the CERCA Program. GG acknowledges an ICREA Academia award from the Institució Catalana de Recerca i Estudis Avançats (ICREA). This work also received funding from the European Commission under Grant Agreement No. H2020-MSCA-721874 (SPM2.0). We acknowledge the MicroFabSpace and Microscopy Characterization Facility, Unit 7 of ICTS “NANBIOSIS” from CIBER at IBEC for the substrate fabrication. L. F. received funding from the European Research Council (grant agreement No. 819417) under the European Union’s Horizon 2020 research and innovation program. We acknowledge G. Gramse, M. A. Edwards and A. Dols-Pérez for earlier work on this topic. We also acknowledge M. Garcia-Parajo for suggestions that inspired the present work.

## REFERENCES

1. Plonsey, R.; Barr, R. C. *Bioelectricity: A Quantitative Approach*; Plenum Press: New York, 1982.
2. Dilger, J. P.; McLaughlin, S. G.; McIntosh, T. J.; Simon, S. A. The dielectric constant of phospholipid bilayers and the permeability of membranes to ions. *Science* **1979**, *206*, 1196-1198.
3. Weaver, J. C.; Chizmadzhev, Y. A. 1996. Theory of electroporation: a review.. *Bioelectrochem. Bioenerg.* **1996**, *41*, 135–160.
4. Olivotto, M.; Arcangeli, A.; Carlà, M.; Wanke, E. Electric fields at the plasma membrane level: A neglected element in the mechanisms of cell signalling. *Bioessays* **1996**, *18*, 495-504.
5. Grimnes, S.; Martinsen, O. *Bioimpedance and bioelectricity basics*; Academic Press: San Diego, 2000.
6. Pohl, H. A. *Dielectrophoresis: The Behavior of Neutral Matter in Nonuniform Electric Fields.*; Cambridge University Press: London, 1978.
7. Jones, T. B. Basic theory of dielectrophoresis and electrorotation. *IEEE Eng. Med. Biol.* **2003**, *22*, 33-42.
8. Hanai, T.; Haydon, D. A.; Taylor, J. The influence of lipid composition and of some adsorbed proteins on the capacitance of black hydrocarbon membranes. *J Theor Biol.* **1965**, *9*, 422-432.
9. Benz, R.; Fröhlich, O.; Läger, P.; Montal, M. Electrical capacity of black lipid films and of lipid bilayers made from monolayers. *Biochim. Biophys. Acta.* **1975**, *394*, 323-334.
10. Naumowicz, M.; Petelska, A. D.; Figaszewski, Z. A. Impedance analysis of phosphatidylcholine–cholesterol system in bilayer lipid membranes. *Electrochim. Acta* **2000**, *50*, 2155-2161.
11. Taylor, G. J.; Heberle, F. A.; Seinfeld, J. S.; Katsaras, J.; Collier, C. P.; Sarles, S. A. Capacitive Detection of Low-Enthalpy, Higher-Order Phase Transitions in Synthetic and Natural Composition Lipid Membranes. *Langmuir* **2017**, *33*, 10016-10026.
12. Velikonja, A.; Kramar, P.; Miklavčič, D.; Maček, L. A. Specific electrical capacitance and voltage breakdown as a function of temperature for different planar lipid bilayers. *Bioelectrochemistry* **2016**, *112*, 132-137.
13. Abraham, S. . H. T.; Morgenstern, Y.; Kaufman, Y. Effect of Temperature on the Structure, Electrical Resistivity, and Charge Capacitance of Supported Lipid Bilayers. *Langmuir* **2019**, *35*, 8709–8715.

14. Naumowicz, M.; Figaszewski, Z. A. The Effect of pH on the Electrical Capacitance of Phosphatidylcholine–Phosphatidylserine System in Bilayer Lipid Membrane. *J. Membrane Biol.* **2014**, *247*, 361–369.
15. Demchenko, A. P.; Mely, Y.; Duportail, G.; Klymchenko, A. S. Monitoring biophysical properties of lipid membranes by environment-sensitive fluorescent probes. *Biophys. J.* **96**, *2009*, 3461-3470.
16. Klymchenko, A. S. Solvatochromic and Fluorogenic Dyes as Environment-Sensitive Probes: Design and Biological Applications. *Acc. Chem. Res.* **2017**, *50*, 366-375.
17. Marsh, D. Polarity and permeation profiles in lipid membranes. *Proc. Natl. Acad. Sci. USA.* **2001**, *98*, 7777-7782.
18. Erilov, D. A.; Bartucci, R.; Guzzi, R.; Shubin, A. A.; Maryasov, A. G.; Marsh, D.; Dzuba, S. A.; Sportelli, L. Water concentration profiles in membranes measured by ESEEM of spin-labeled lipids. *J. Phys. Chem. B* **2005**, *109*, 12003-12013.
19. Guzzi, R.; Bartucci, R. Electron spin resonance of spin-labeled lipid assemblies and proteins. *Arch. Biochem. Biophys.* **2015**, *580*, 102-111.
20. Botet-Carreras, A.; Montero, M. T.; Domènech, O.; Borrell, J. H. Effect of cholesterol on monolayer structure of different acyl chained phospholipids. *Colloids Surf. B: Biointerfaces* **2019**, *174*, 374-383.
21. Ohki, S. The electrical capacitance of phospholipid membranes.. *Biophys. J.* **1969**, *9*, 1195–1205.
22. Ashcroft, R. G.; Coster, H. G. L.; Laver, D. R.; Smith, J. R. The effects of cholesterol inclusion on the molecular organisation of bimolecular lipid membranes. *Biophys. Biochim. Acta - Biomembr.* **1983**, *730*, 231–238.
23. Naumowicz, M.; Petelska, A. D.; Figaszewski, Z. A. Capacitance and resistance of the bilayer lipid membrane formed of phosphatidylcholine and cholesterol. *Cell. Mol. Biol. Lett.* **2003**, *8*, 5-18.
24. Naumowicz, M.; Figaszewski, Z. A. Impedance analysis of lipid domains in phosphatidylcholine bilayer membranes containing ergosterol. *Biophys. J.* **2005**, *89*, 3174–3182.
25. Karolis, C.; Coster, H. G. L.; Chilcott, T. C.; Barrow, K. D. Differential effects of cholesterol and oxidised-cholesterol in egg lecithin bilayers. *Biochim. Biophys. Acta - Biomembr.* **1998**, *1368*, 247–255.
26. Abraham, S.; Heckenthaler, T.; Bandyopadhyay, D.; Morgenstern, Y.; Kaufman, Y. Quantitative Description of the Vesicle Fusion Mechanism on Solid Surfaces and the Role of

- Cholesterol. *J. Phys. Chem. C* **2018**, *122*, 22985-22995.
27. Alobeedallah, H.; Cornell, B.; Coster, H. The Effect of Cholesterol on the Dielectric Structure of Lipid Bilayers. *J. Membr. Biol.* **2018**, *251*, 153–161.
  28. Coster, H. G. L. Dielectric and Electrical Properties of Lipid Bilayers in Relation to their Structure. In *Planar Lipid Bilayers (BLMs) and Their Applications*; Tien, H. T., Ottova-Leitmannova, A., Eds.; Elsevier Science: Amsterdam, 2003; Vol. 7, pp 75-108.
  29. Sukhorukov, V. L.; Arnold, W. M.; Zimmermann, U. Hypotonically Induced Changes in the Plasma Membrane of Cultured Mammalian Cells. *J. Membrane Biol.* **1993**, *132*, 27-40.
  30. Asami, K.; Takahashi, Y.; S., T. Frequency domain analysis of membrane capacitance of cultured cells (HeLa and myeloma) using the micropipette technique. *Biophys. J.* **1990**, *58*, 143-148.
  31. Solsona, C.; Innocenti, B.; Fernández, J. M. Regulation of exocytotic fusion by cell inflation. *Biophys. J.* **1998**, *74*, 1061-1073.
  32. Gentet, L. J.; Stuart, G. J.; Clements, J. D. Direct measurement of specific membrane capacitance in neurons. *Biophys. J.* **2000**, *79*, 314–320.
  33. White, S. H. The Physical Nature of Planar Bilayer Membranes. In *Ion Channel Reconstitution*; Miller, C., Ed.; Springer: Boston, 1986; pp 3-35.
  34. Coster, H. G. L.; Chilcott, T. C.; F., C. A. C. Impedance spectroscopy of interfaces, membranes and ultrastructures. *Bioelectrochem. Bioener.* **1996**, *40*, 79-98.
  35. Kalinowski, S. Electrochemical Methods and Their Application. In *Advances in Planar Lipid Bilayers and Liposomes*; Ottova-Leitmannova, A., Ed.; Academic Press: San Diego, 2005; Vol. 2, pp 1-47.
  36. Gross, L. C.; Heron, A. J.; Baca, S. C.; Wallace, M. I. Determining membrane capacitance by dynamic control of droplet interface bilayer area. *Langmuir* **2011**, *27*, 14335-14342.
  37. Asami, K. Dielectric imaging of biological cells. *Colloid. Polym. Sci.* **1995**, *273*, 1095-1097.
  38. Fumagalli, L.; Ferrari, G.; Sampietro, M.; Gomila, G. Quantitative Nanoscale Dielectric Microscopy of Single-Layer Supported Biomembranes. *Nano Lett.* **2009**, *9*, 1604-1608.
  39. Fumagalli, L.; Esteban-Ferrer, D.; Cuervo, A.; Carrascosa, J. L.; Gomila, G. Label-free identification of single dielectric nanoparticles and viruses with ultraweak polarization forces. *Nat. Mater.* **2012**, *11*, 808–816.
  40. Gomila, G.; Toset, J.; Fumagalli, L. Nanoscale capacitance microscopy of thin dielectric films. *J. Appl. Phys.* **2008**, *104*, 024315.

41. Gomila, G.; Gramse, G.; Fumagalli, F. Finite-size effects and analytical modeling of electrostatic force microscopy applied to dielectric films. *Nanotechnology* **2014**, *25*, 255702.
42. Gramse, G.; Edwards, M. A.; Fumagalli, L.; Gomila, G. . Dynamic electrostatic force microscopy in liquid media. *Appl. Phys. Lett.* **2012**, *101*, 213108.
43. Gramse, G.; Dols-Perez, A.; Edwards, M. A.; Fumagalli, L.; Gomila, G. Nanoscale measurement of the dielectric constant of supported lipid bilayers in aqueous solutions with electrostatic force microscopy. *Biophys. J.* **2013**, *104*, 1257-1262.
44. Gramse, G.; Edwards, M. A.; Fumagalli, L.; Gomila, G. Theory of amplitude modulated electrostatic force microscopy for dielectric measurements in liquids at MHz frequencies. *Nanotechnology* **2013**, *24*, 415709.
45. Millan-Solsona, R.; Checa, M.; Fumagalli, L.; Gomila, G. Mapping the capacitance of self-assembled monolayers at metal/electrolyte interfaces at the nanoscale by in-liquid scanning dielectric microscopy. *Nanoscale* **2020**, doi.org/10.1039/D0NR05723A.
46. Basu, A.; Karmakar, P.; Karmakar, S. Supported planar single and multiple bilayer formation by DOPC vesicle rupture on mica substrate: a mechanism as Revealed by atomic force microscopy study. *J. Membrane Biol.* **2020**, *253*, 2020.
47. Regan, D.; Williams, J.; Borri, P.; Langbein, W. Lipid bilayer thickness measured by quantitative DIC reveals phase transitions and effects of substrate hydrophilicity. *Langmuir* **2019**, *35*, 13805–13814.
48. Kučerka, N.; Pencser, J.; Nieh, M.-P.; Katsaras, J. Influence of cholesterol on the bilayer properties of monounsaturated phosphatidylcholine unilamellar vesicles. *Eur. Phys. J. E* **2007**, *23*, 247–254.
49. Chakraborty, S.; Doktorova, M.; Molugu, T. R.; Heberle, F. A.; Scott, H. L.; Dzikovski, B.; Nagao, M.; Stingaciu, L.-R.; Standaert, R. F.; Barrera, F. N.; Katsaras, J.; Khelashvili, G.; Brown, M. F.; Ashkar, R. How cholesterol stiffens unsaturated lipid membranes. *Proc. Natl. Acad. Sci. USA* **2020**, doi:10.1073/pnas.2004807117.
50. Fumagalli, L.; Esfandiar, A.; Fabregas, R.; Hu, S.; Ares, P.; Janardanan, A.; Yang, Q.; Radha, B.; Taniguchi, T.; Watanabe, K.; Gomila, G.; Novoselov, K. S.; Geim, A. K. Anomalously low dielectric constant of confined water. *Science* **2018**, *360*, 1339-1342.
51. Pan, J.; Mills, T. T.; Tristram-Nagle, S.; Nagle, J. F. Cholesterol Perturbs Lipid Bilayers Nonuniversally. *Phys. Rev. Lett.* **2008**, *100*, 198103.
52. Dols-Perez, A.; Fumagalli, L.; Gomila, G. Structural and nanomechanical effects of cholesterol in binary and ternary spin-coated single lipid bilayers in dry conditions. *Colloids. Surf. B Biointerfaces* **2014**, *116*, 295-302.

53. Hung, W.-C.; Lee, M.-T.; Chen, F. H.; Huang, H. W. The condensing effect of cholesterol in lipid bilayers. *Biophys. J.* **2007**, *92*, 3960–3967.
54. Dols-Perez, A.; Gramse, G.; Calo, A.; Gomila, G.; Fumagalli, L. Nanoscale electric polarizability of ultrathin bilayers on insulator substrates by electrostatic force microscopy. *Nanoscale* **2015**, *7*, 18327-18336.
55. Huang, J.; Feigenson, G. W. A microscopic interaction model of maximum solubility of cholesterol in lipid bilayers. *Biophys J.* **1999**, *76*, 2142-2157.
56. Engelman, D. M. Membranes are more mosaic than fluid. *Nature* **2005**, *438*, 578.
57. Sezgin, E.; Levental, I.; Mayor, S.; Eggeling, C. The mystery of membrane organization: composition, regulation and roles of lipid rafts. *Nat. Rev. Mol. Cell. Biol.* **2017**, *18*, 361-374.
58. Théry, C.; Zitvogel, L.; Amigorena, S. Exosomes: composition, biogenesis and function. *Nat. Rev. Immunol.* **2002**, *2*, 569–579.
59. Schwechheimer, C.; Kuehn, M. Outer-membrane vesicles from Gram-negative bacteria: biogenesis and functions. *Nat. Rev. Microbiol.* **2015**, *13*, 605–619.
60. Pirbadian, S.; Barchinger, S. E.; Leung, K. M.; Byun, H. S.; Jangir, Y.; Bouhenni, R. A.; Reed, S. B.; Romine, M. F.; Saffarini, D. A.; Shi, L.; Gorby, Y. A.; Golbeck, J. H.; El-Naggar, M. Y. *Shewanella oneidensis* MR-1 nanowires are outer membrane and periplasmic extensions of the extracellular electron transport components. *Proc. Natl Acad. Sci. USA* **2014**, *111*, 12883–12888.
61. Fumagalli, L.; Gramse, G.; Esteban-Ferrer, D.; Edwards, M. A.; Gomila, G. Quantifying the dielectric constant of thick insulators using electrostatic force microscopy. *Appl. Phys. Lett.* **2010**, *96*, 183107.
62. Checa, M.; Millan-Solsona, R.; Gomila, G. Frequency-dependent force between ac voltage biased plates in electrolyte solutions. *Phys. Rev. E* **2019**, *100*, 022604.
63. Gramse, G.; Gomila, G.; Fumagalli, L. Quantifying the dielectric constant of thick insulators by electrostatic force microscopy: effects of the microscopic parts of the probe. *Nanotechnology* **2012**, *23*, 205703.

TOC

